Washington University in St. Louis
Washington University Open Scholarship

Mechanical Engineering and Materials Science Independent Study

Mechanical Engineering & Materials Science

5-9-2024

Elastic Fiber Fragmentation in the Descending Aortic Wall of mgR/mgR Model Marfan Syndrome Mice

Maya Sumra
Washington University in St. Louis

Follow this and additional works at: https://openscholarship.wustl.edu/mems500

Recommended Citation

Sumra, Maya, "Elastic Fiber Fragmentation in the Descending Aortic Wall of mgR/mgR Model Marfan Syndrome Mice" (2024). *Mechanical Engineering and Materials Science Independent Study*. 266.
https://openscholarship.wustl.edu/mems500/266

This Final Report is brought to you for free and open access by the Mechanical Engineering & Materials Science at Washington University Open Scholarship. It has been accepted for inclusion in Mechanical Engineering and Materials Science Independent Study by an authorized administrator of Washington University Open Scholarship. For more information, please contact digital@wumail.wustl.edu.

ABSTRACT

Aortic aneurysms often lead to death due to aortic wall dissections and ruptures, which are caused by weakness and fragmentation in the elastin-composed elastic fibers of the extracellular matrix; because of a genetic mutation affecting connective tissue structure, these aneurysms are especially prevalent in individuals with Marfan syndrome. This study hypothesized that elastic fiber fragmentation in the descending aortic wall is greater for mgR/mgR model Marfan syndrome mice than wild type mice. It also aimed to observe differences in fragmentation among mouse ages and sexes. The results showed no increase in fragmentation for mgR/mgR mice and no changes in fragmentation among ages or sexes. Each group with varying age, sex, and genotype was represented by one sample in the study, therefore more research must be conducted to thoroughly assess the hypothesis.

INTRODUCTION

Aortic aneurysms occur when the aorta—the largest blood vessel in the human body, which supplies blood from the heart to other arteries—circumferentially expands in a localized area. These can lead to aortic dissections, tears in the inner aortic wall, and ruptures that frequently lead to death. When these aneurysms develop in the thorax, or chest, they are referred to as thoracic aortic aneurysms (TAAs) [1]. The main segments of the aorta in the thorax are the ascending and descending aorta; the ascending aorta is the part of the vessel that accepts blood pumped from the heart, and the descending aorta contains the downstream end of blood flow, distributing blood to arteries in the lower portion of the body. Without surgery, aortic wall ruptures caused by TAAs have mortality rates over 94% [2]. The aortic wall expansion that characterizes TAAs occurs when the aortic wall becomes weak; when it is weaker, the vessel undergoes greater amounts of stress due to blood flow pressure, which increases circumferential strain and expands the aortic wall. These weaknesses can develop because of plaque buildup and calcification, infections, and genetic conditions: Marfan syndrome (MFS) is one such condition. Individuals with MFS are predisposed to aortic wall weaknesses because of genetic mutations affecting the structure of connective tissue in the body [3]. These mutations affect the assembly and cross-linking of elastic fibers in the aortic wall's extracellular matrix (ECM) [4].

The protein that gives aortic walls elasticity is called elastin; in the ECM, elastin cross-links with other proteins to form elastic laminae, giving the aorta its elastic response to

blood pressure and thereby its resistance to dilation [5]. In aortae with TAAs, these elastic fibers become disorganized—fragmentation is the term used to describe the disorganization of elastic fibers [4]. The fibrillin-1 gene allows for proper elastic fiber formation and is mutated in those with MFS, which affects elastic fiber assembly and cross-linking. This causes fragmentation, explaining why the disorder can lead to TAAs. With increasingly fragmented elastic laminae, the aortic wall has dampened elastic responses and is more prone to dissections and ruptures [5].

Fragmentation is characterized by four variables that can be quantified for aortae using microscopy and image analysis: junctions, end points, branches, and slabs. A labeled visualization of these terms is shown in Fig. 1.

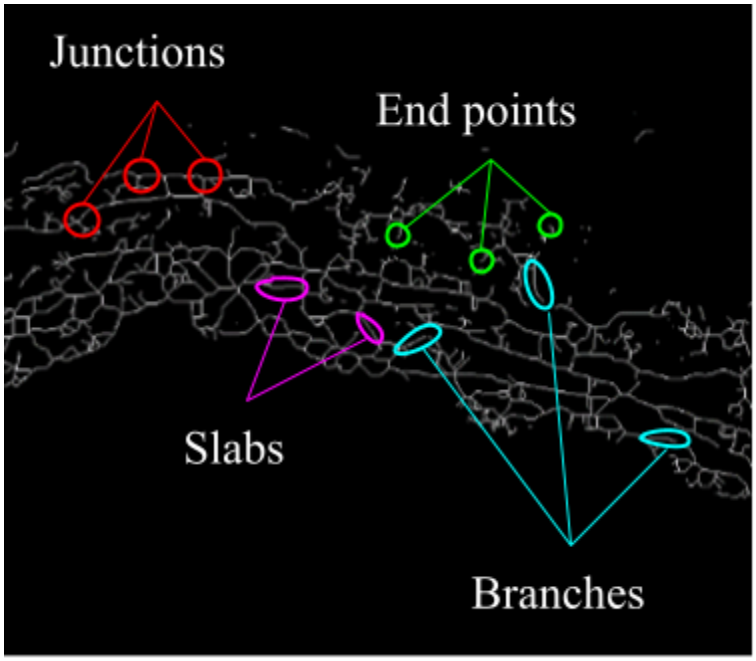

Figure 1. Fragmentation characteristics. A maximum-intensity, binary skeleton of elastic fibers (white laminae) in an aortic wall sample is shown. *Junctions*: white pixels with three or more neighbors—locations where three or more fibers meet (circled in red). *End points*: white pixels with either one neighbor or zero— locations where fibers discontinue (circled in green) [4]. *Branches*: strands of white pixels connecting junctions and end points. *Slabs*: remaining pixel strands with exactly two neighbors [6].

Junctions, end points, and slabs can also be counted in terms of voxels, which are 3D pixels with height dimensions equal to the spacing between each image in the Z-stack that was superimposed to generate a maximum-intensity image. An increase in fragmentation correlates to an increase in junctions, branches, end points, and slabs, along with their voxel counterparts. It also correlates to a decrease in average branch length and maximum branch length.

Although aneurysms form in the ascending aorta, mechanical changes in the aortic wall due to TAA development also occur in the descending aorta (DSC) [7]. This study will determine if these mechanical changes in the DSC are related to elastic fiber fragmentation in the aortic wall. Fragmentation will be quantified for wild type mice and mgR/mgR model Marfan syndrome mice, with the hypothesis that fragmentation is greater for mutant (mgR/mgR) mice than wild type mice. The fibrillin-1 gene in mgR/mgR mice is underexpressed due to the mgR gene-targeting mutation; these mice develop and experience aortic aneurysms with characteristics similar to MFS [8]. TAAs originating from fibrillin-1 mutations have been found to cause elastic fiber fragmentation, and since mgR/mgR mice possess this mutation, we expect fragmentation to be greater for the model MFS mutant mice [9]. This study also aims to determine whether there are differences in fragmentation among sexes or the ages at which TAAs develop in the ascending aorta (1-4 months).

METHODS

To collect data for this study, one sample of mouse DSC from the thorax was prepared for each combination of factors: genotype, age, and sex. The genotype factor had two levels, mgR/mgR model MFS (the mutant group, MU) and wild type (WT); age had four levels, 1-4 months; and sex had two levels, male and female. This resulted in 16 groups, each representing a unique combination of factors. First, the samples were cut into small rings, mounted in optimal cutting-temperature (OCT) compound, and frozen to -80℃. Once frozen, each sample was sectioned into 10 μm-thick slices in a -20℃ cryostat and placed on a glass slide. The slides were placed back in the -80℃ freezer to ensure proper adherence, and fluorescent DAPI stain and coverslips were applied.

After preparation, the samples were imaged for elastin and collagen with a Leica SP8-DIVE multiphoton microscope. Each sample was placed under a 25x-zoom water immersion lens and the position was adjusted so that only the clearest part of the descending aortic wall was in view. A Z-stack image series was taken for each sample, capturing the elastin and collagen levels approximately every 1 μm throughout the samples' depth. In the Leica LAS X software, collagen was identified at 440 nm and elastin between 500-600 nm; the signals appeared red and green, respectively.

The Z-stacks were analyzed in ImageJ software by generating one maximum-intensity image per sample, isolating the elastin signals, converting the images to binary, and skeletonizing them with the AnalyzeSkeleton function. This converted each binary image into discrete vectors representing the elastic fibers in the aortic walls [6]. Figure 2 shows a sample skeletonized image and describes the skeletonization procedure.

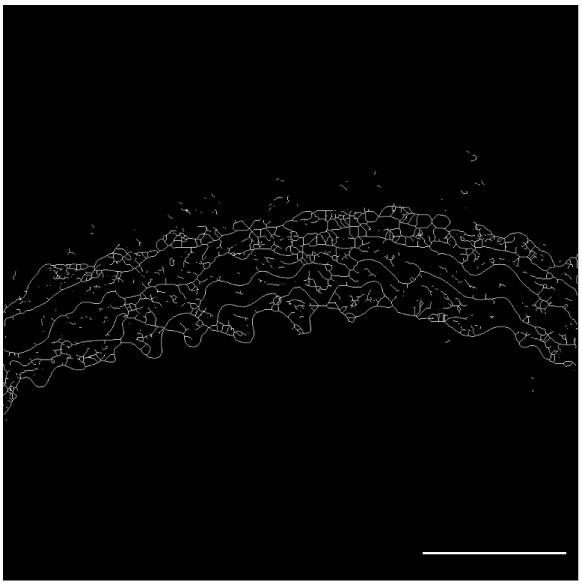

Figure 2. Skeletonized image, 3 month MU female. All intensities in the Z-stack were superimposed and the RGB channels were split to isolate the green channel containing elastin signals. The areas of these regions were carefully traced and recorded, in pixels. The image threshold was adjusted to reduce visible interference in the ECM and to see the laminae more clearly. Images were despeckled and made binary. AnalyzeSkeleton was applied, pruning short branches and eliminating their ends. Scale bar ≈100 μm.

For each of the 16 skeletonized images, ImageJ recorded the number of junctions, branches, junction voxels, end point voxels, slab voxels, the average branch length, and the maximum branch length. Excel was used to average the data points at each pixel or voxel for the stated quantities, except for maximum branch length—instead, the maximum of those data were taken. All the results were normalized by the respective areas and bar graphs of each quantity and all combinations were generated in Matlab.

RESULTS & DISCUSSION

Figure 3 shows the multiphoton microscope images of DSC aortic walls taken for all genotype (MU, WT), age (1-4 months), and sex (male, female) combinations.

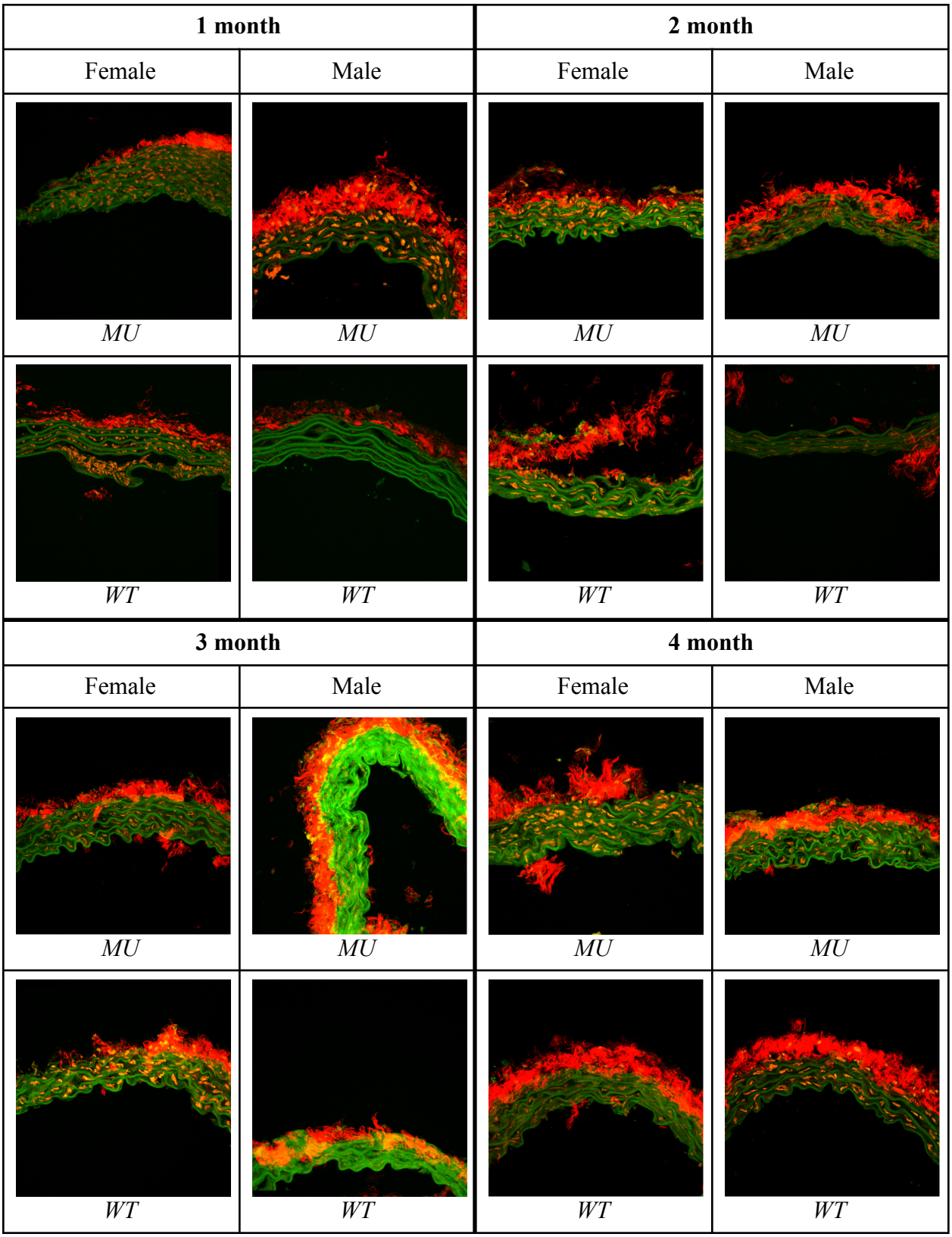

Figure 3. Multiphoton microscope images. The green laminae in the images are the elastic fibers in the ECM. The red layers represent collagen in the outer layer of the aortic wall, the adventitia. Orange cells between the elastic fibers are interferences from cell nuclei due to the DAPI stain.

In Figure 3, an inconsistency among samples is evident in the 1 month WT male because no DAPI stain was applied, which caused the absence of orange interferences in the image. Additionally, in some of the samples, such as the 2 month WT female and male, the collagen layer has separated from the aortic wall; this is likely because of sample preparation issues. It is also evident that the 3 month MU male image is significantly more intense than the other images; this intensity setting was applied in the LAS X software to see the laminae better. Figure 4 shows the results for the average number of junctions and branches from ImageJ, for all genotypes, ages, and sexes.

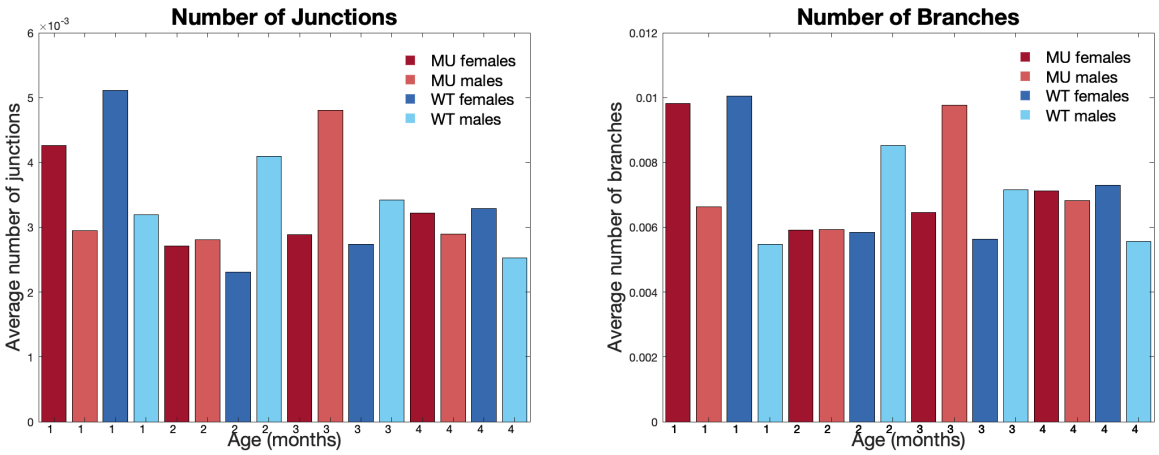

A **B**

Figure 4. Average number of junctions (*A*) and branches (*B*) for all samples. Shades of red represent MU groups. Shades of blue represent WT groups. The darker shade for each color represents females (dark red and dark blue) while the lighter color represents males (pink and light blue).

Neither of the graphs for the average number of junctions and branches for each sample show a relationship between age or sex. It is clear that the values fluctuate among ages, and among sexes. Additionally, the results do not seem to support the hypothesis that fragmentation is greater for the mutants (the shades of red). If this were the case, we would observe the red bars being higher than the blue bars, indicating more junctions and branches. Figure 5 shows the results for the average number of junction, end point, and slab voxels in each of the samples.

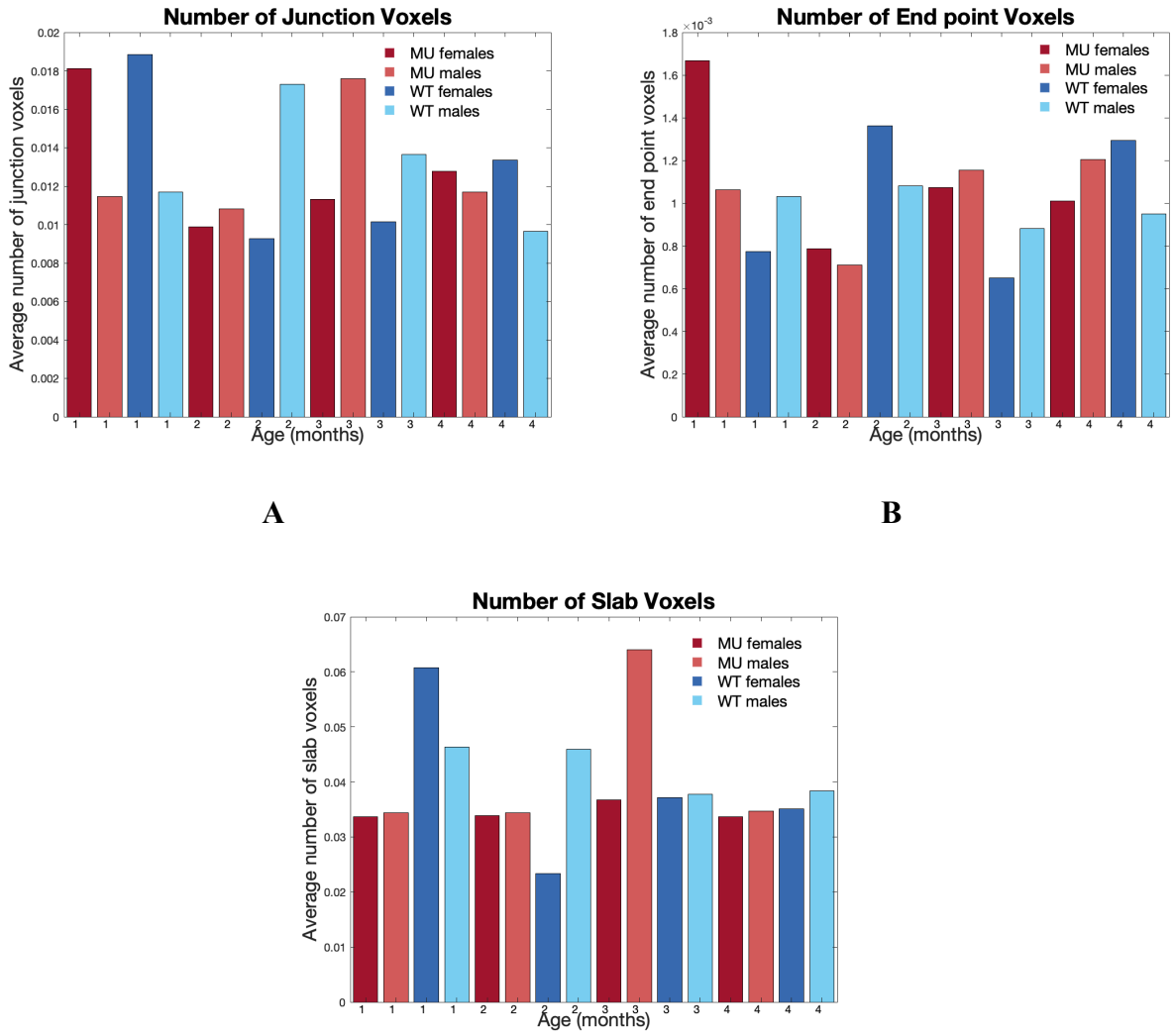

Figure 5. Average number of junction (*A*), end point (*B*), and slab (*C*) voxels for all samples. Shades of red represent MU groups. Shades of blue represent WT groups. The darker shade for each color represents females (dark red and dark blue) while the lighter color represents males (pink and light blue).

None of the results show a visually significant relationship between ages or sexes for the average number of junction voxels, end point voxels, and slab voxels: the values fluctuate among ages, and bars for the dark shades do not appear higher than the light shades. Overall, the average number of junction voxels in the samples is not greater for mutants, which does not support the hypothesis. However, the end point voxel results may support the hypothesis because it is clear that the 1 and 3 month mutant samples have more end point voxels than the wild type mice at their respective ages. The slab voxel results may also support the hypothesis because the 3 month

mutants appear to have more slab voxels than the 3 month wild type mice. Since each group has only one sample, it is not valid to run statistical analyses, therefore the most powerful conclusions we may draw are that the data may or may not support the hypothesis. Figure 6 shows the results for the samples' average and maximum branch lengths.

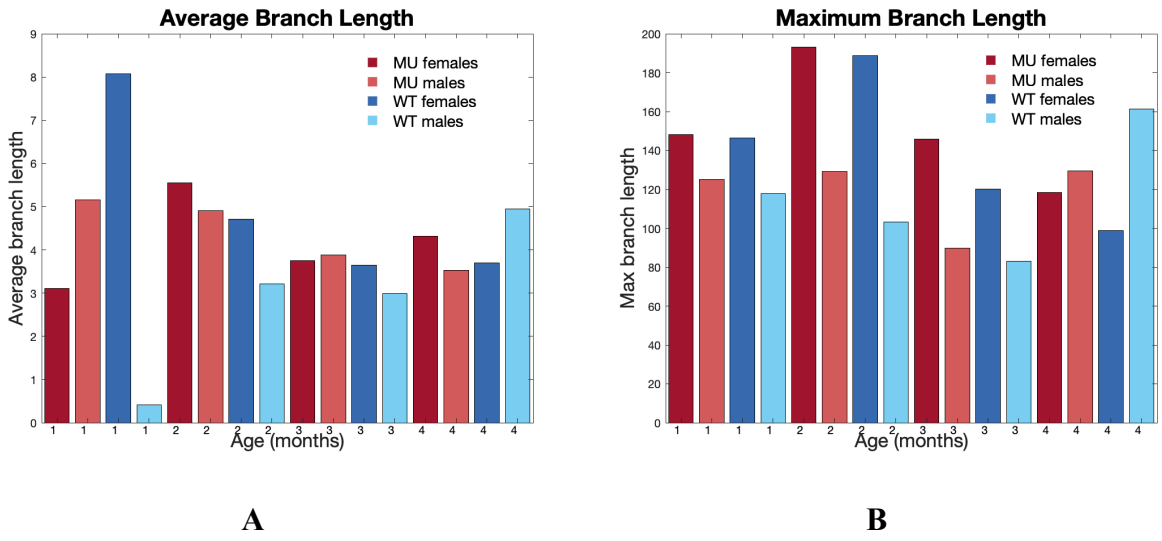

Figure 6. Average (*A*) and maximum (*B*) branch lengths for all samples, in pixels. Shades of red represent MU groups. Shades of blue represent WT groups. The darker shade for each color represents females (dark red and dark blue) while the lighter color represents males (pink and light blue).

In Figure 6A, it is evident that the 1 month WT male is an outlier because its branch length is extremely low compared to the other samples. The image processing and skeletonizing settings for this sample were correct, and the data file shows that the only quantity with unusual values is the average branch length. By visual inspection of the skeletonized image, there seems to be more short fibers and specks than in other samples, explaining why the average branch length is very small but maximum branch length is closer to the other samples. The large number of very short branches could be due to threshold settings not excluding enough interference, but referring back to Figure 3, no DAPI was applied to this sample, which dramatically reduced interference in the ECM. Therefore, it is more likely that the average branch length of the 1 month WT male is accurate and the same data for the remaining samples are magnified due to DAPI.

There does not appear to be an overall relationship between sex and average branch length or maximum branch length. There also doesn't seem to be a relationship between ages and

maximum branch length, but there is a potential decrease in average branch length with increasing age. Both the maximum and average branch length results show that those quantities are higher for mutant males than wild type males. This contradicts the hypothesis of increased fragmentation for mutants because if mutants have greater levels of fragmentation than wild type mice, we should expect that they have shorter average and maximum branch lengths.

One source of error in this study is the variation in threshold settings for image analysis. To see the elastic fibers as clearly as possible and minimize noise from DAPI in the ECM, the threshold setting was slightly different for every sample. This contributes to the variation between results. Additionally, each sample had different amounts of interference from DAPI because of the varying number of cell nuclei visible in each image. The general quality of samples could have also been affected by preparation techniques, such as cryostat sectioning. Finally, the sample size of $n = 1$ per group restricted the possibility of having more accurate data to analyze and running statistical tests.

CONCLUSION

This study found no clear increase in elastic fiber fragmentation in the descending aorta for mgR/mgR model Marfan syndrome mice compared to wild type mice. The results for the average number of slab voxels and end point voxels may suggest that the mgR/mgR mice have more fragmented descending aortic walls. The study also found that there is no overall change in fragmentation between the mouse TAA development ages of 1-4 months or between sexes, although there may be a decrease in average branch length with increasing age. A larger sample size for each group would be required to perform statistical tests and further evaluate the effects of age, sex, and genotype on fragmentation. With a greater sample size, one-way analysis of variance (ANOVA) tests can be conducted for each factor of interest, which would allow us to determine if there is significant variance between age, sex, and genotype for the average number of branches, junctions, junction voxels, end point voxels, slab voxels, average branch length, and maximum branch length in descending aortic walls.

References

[1] “Aortic Aneurysm.” *Mayo Clinic*, Mayo Foundation for Medical Education and Research, 21 Apr. 2023, www.mayoclinic.org/diseases-conditions/aortic-aneurysm/symptoms-causes/syc-20369472. Accessed 15 Apr., 2024.

[2] Olsson, Christian, et. al. “Thoracic Aortic Aneurysm and Dissection Increasing Prevalence and Improved Outcomes Reported in a Nationwide Population-Based Study of More Than 14 000 Cases From 1987 to 2002.” *Circulation*, vol. 144, no. 24, 12 Dec. 2006, https://doi.org/10.1161/CIRCULATIONAHA.106.630400.

[3] “Thoracic Aortic Aneurysm.” *Mayo Clinic*, Mayo Foundation for Medical Education and Research, 25 Apr. 2023, www.mayoclinic.org/diseases-conditions/thoracic-aortic-aneurysm/symptoms-causes/syc-20350188#:~:text=A%20thoracic%20aortic%20aneurysm%20is,artery%20is%20called%20the%20aorta. Accessed 15 Apr., 2024.

[4] Crandall, Christie L., et al. “Changes in transmural mass transport correlate with ascending thoracic aortic aneurysm diameter in a fibulin-4 E57K Knockin Mouse model.” *American Journal of Physiology-Heart and Circulatory Physiology*, vol. 325, no. 1, 2 June 2023, https://doi.org/10.1152/ajpheart.00036.2023.

[5] Cocciolone, Austin J., et al. “Elastin, arterial mechanics, and cardiovascular disease.” *American Journal of Physiology-Heart and Circulatory Physiology*, vol. 315, no. 2, 1 Aug. 2018, https://doi.org/10.1152/ajpheart.00087.2018.

[6] “AnalyzeSkeleton.” *ImageJ*, 24 Jan. 2020, imagej.net/imagej-wiki-static/AnalyzeSkeleton. Accessed 15 Apr., 2024.

[7] Tsamis, Alkiviadis, et al. “Elastin and collagen fibre microstructure of the human aorta in Ageing and disease: A review.” *Journal of The Royal Society Interface*, vol. 10, no. 83, 6 June 2013, p. 20121004, https://doi.org/10.1098/rsif.2012.1004.

[8] Pereira, L et al. “Pathogenetic sequence for aneurysm revealed in mice underexpressing fibrillin-1.” *Proceedings of the National Academy of Sciences of the United States of America* vol. 96,7 (1999): 3819-23. doi:10.1073/pnas.96.7.3819.

[9] Chen, Jeff Z., et al. “Aortic strain correlates with elastin fragmentation in fibrillin-1 hypomorphic mice.” *Circulation Reports*, vol. 1, no. 5, 10 May 2019, pp. 199–205, https://doi.org/10.1253/circrep.cr-18-0012.